A multiomics approach reveals RNA dynamics promote cellular sensitivity to DNA hypomethylation

Alex Y. Ge[1,#], Abolfazl Arab[2,3,4,#], Raymond Dai[2,3,4,#], Albertas Navickas[3,4,5,6], Lisa Fish[3,4,5,6], Kristle Garcia[3,4,5,6] , Hosseinali Asgharian[3,4,5,6], Jackson Goudreau[2], Sean Lee[3,4,5,6], Kathryn Keenan[7], Melissa B. Pappalardi[7], Michael T. McCabe[7], Laralynne Przybyla[5,8], Hani Goodarzi[2,3,4,5,6,*], Luke A. Gilbert[2,3,4*]

1 School of Medicine, University of California, San Francisco, San Francisco, CA 94158, USA
2 Arc Institute, Palo Alto, CA 94304, USA
3 Department of Urology, University of California, San Francisco, San Francisco, CA 94158, USA
4 Helen Diller Family Comprehensive Cancer Center, University of California, San Francisco, San Francisco, CA 94158, USA
5 Department of Biochemistry and Biophysics, University of California, San Francisco, San Francisco, CA 94158, USA
6 Bakar Computational Health Sciences Institute, University of California, San Francisco, San Francisco, CA 94158, USA
7 Tumor Cell Targeting Research Unit, Research, GSK, Collegeville, PA 19426, USA
8 Laboratory for Genomics Research, San Francisco, CA 94158, USA

#Equal contribution and co-first authors
*Co-correspondence: Hani@arcinstitute.org and Luke@arcinstitute.org

SUPPLEMENTARY FIGURES

Supplementary Figure 1. HL-60i validation and analysis of decitabine induced CpG DNA methylation changes in a public dataset

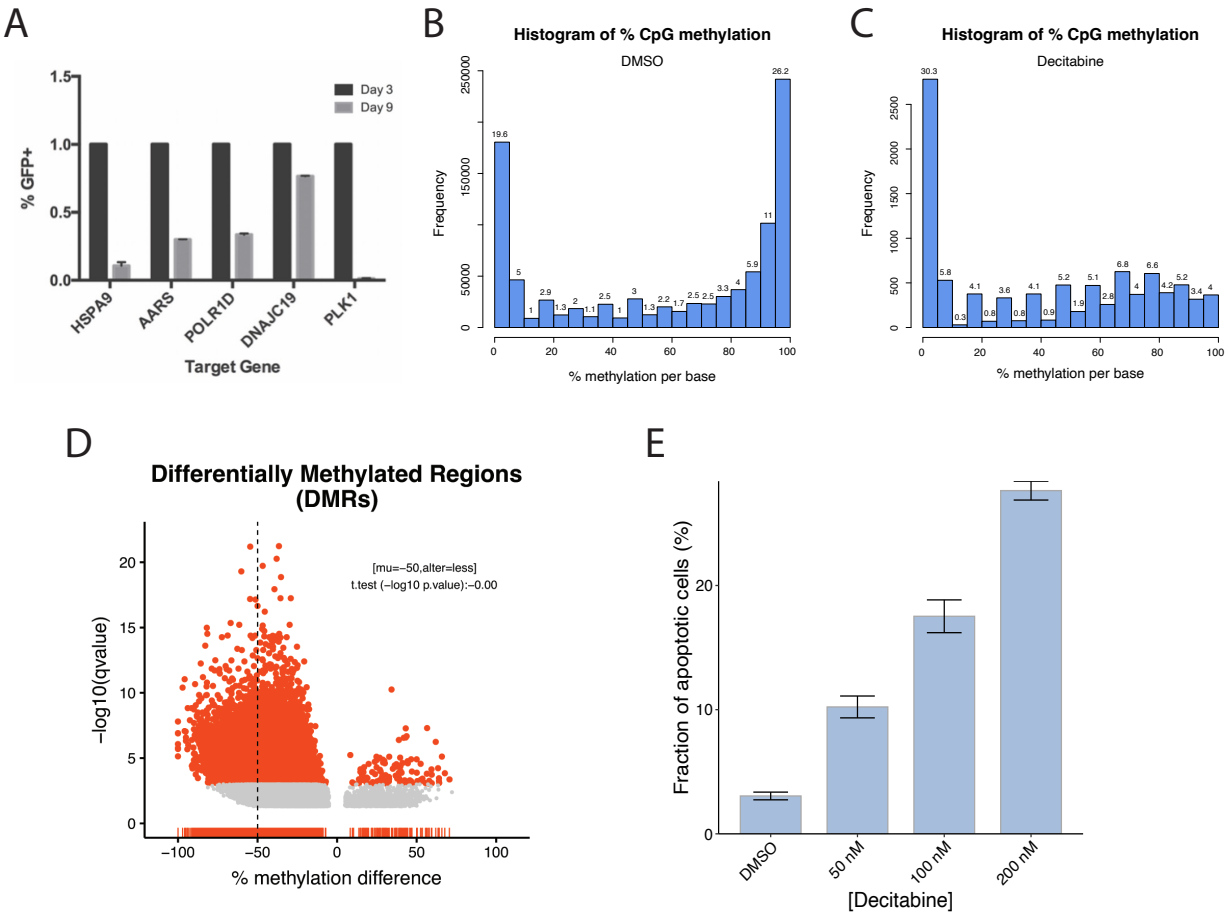

(**a**) Relative depletion of five sgRNAs targeting essential genes at day 9 (relative to day 3) in the HL-60i cell line, demonstrating functional CRISPRi activity. Each sgRNA was introduced into HL-60i via lentiviral transduction at infection rates of ~5–20%. GFP expression was used as a surrogate for sgRNA expression and the starting infection percentage for each sgRNA was normalized to 1. Cells were monitored over time via flow cytometry. Data are shown as means ± SD for two replicates. (**b-d**) Reanalysis of a public bisulfite-sequencing dataset (GSE149954) showing frequencies of base resolution CpG methylation in HL-60 cells treated with (**b**) DMSO or (**c**) 300 nM decitabine. (**d**) Volcano plot of differentially methylated regions (DMRs) comparing cells treated with decitabine vs. DMSO. A one-sided t-test shows statistically significant global hypomethylation of DNA CpG islands. (**e**) Apoptosis assay measuring cleaved caspase 3/7 at day 5 following treatment with DMSO or decitabine. Data are shown as means ± SD for three replicates. Data were derived from the same experiment as Figure 1G.

Supplementary Figure 2. CRISPRi decitabine screen phenotype score metrics and quality control analysis for HL-60 screen

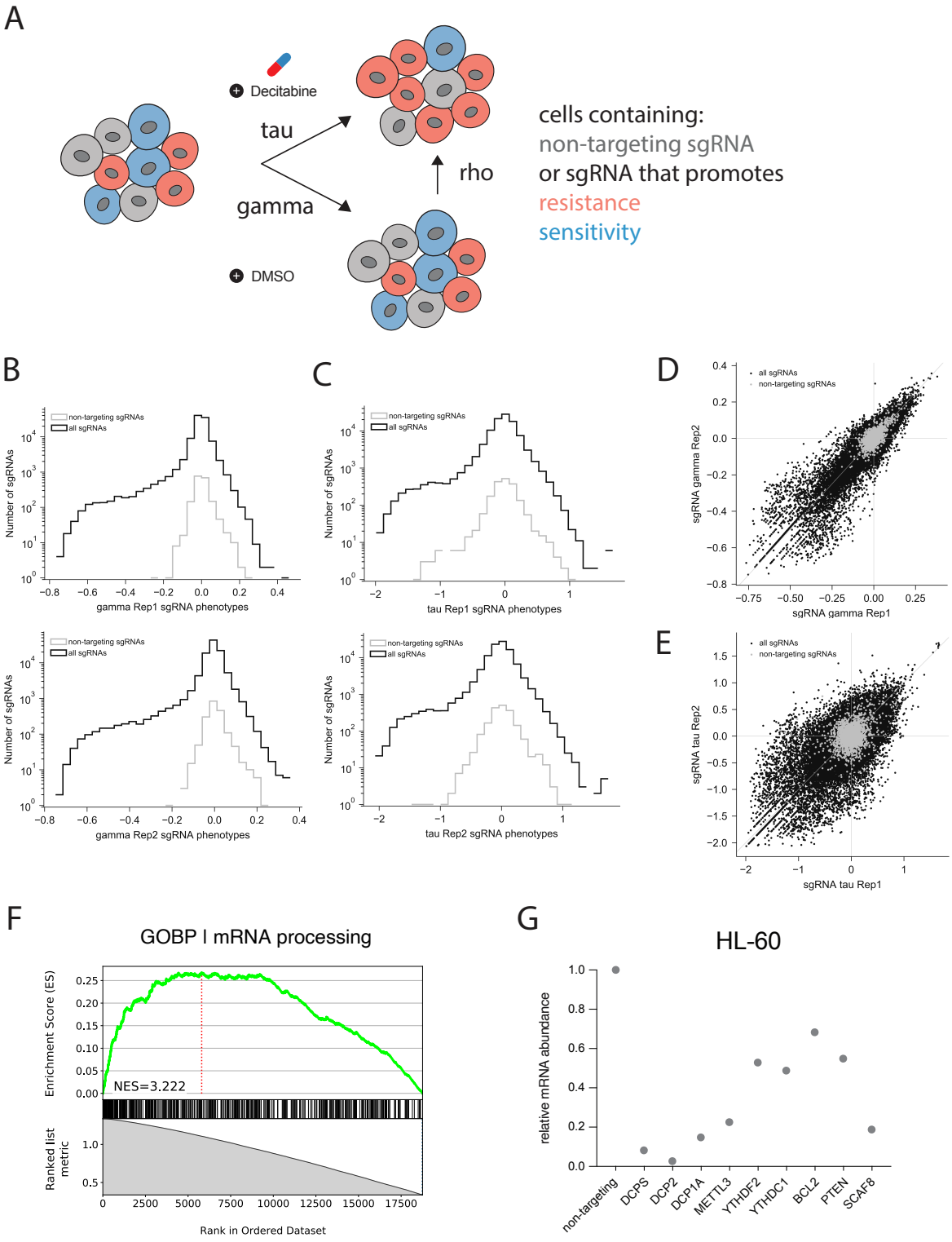

(**a**) Definition of CRISPRi screen phenotypes. (**b-d**) Distributions of sgRNA phenotypes per each HL-60 screen replicate show many sgRNAs are highly active relative to the negative control sgRNA distribution. (**d-e**) Scatter plots show robust correlation between HL-60 screen replicates for the gamma and tau phenotypes. Targeting and non-targeting sgRNAs included in the library are color coded black and gray, respectively. **(f)** GSEA plot showing enrichment of GO:0006397 (mRNA processing) among all screened genes ranked by Mann-Whitney p-value (corresponding to each gene's ρ phenotype calculation). Normalized enrichment scores (NES) were calculated using the blitzGSEA Python package. (**g**) CRISPRi knockdown levels of nine hit genes in HL-60 cells. Data are plotted as mRNA abundance for each gene-targeting sgRNA relative to a non-targeting control sgRNA.

Supplementary Figure 3. Characterizing synergy between decitabine and RG3039 in AML

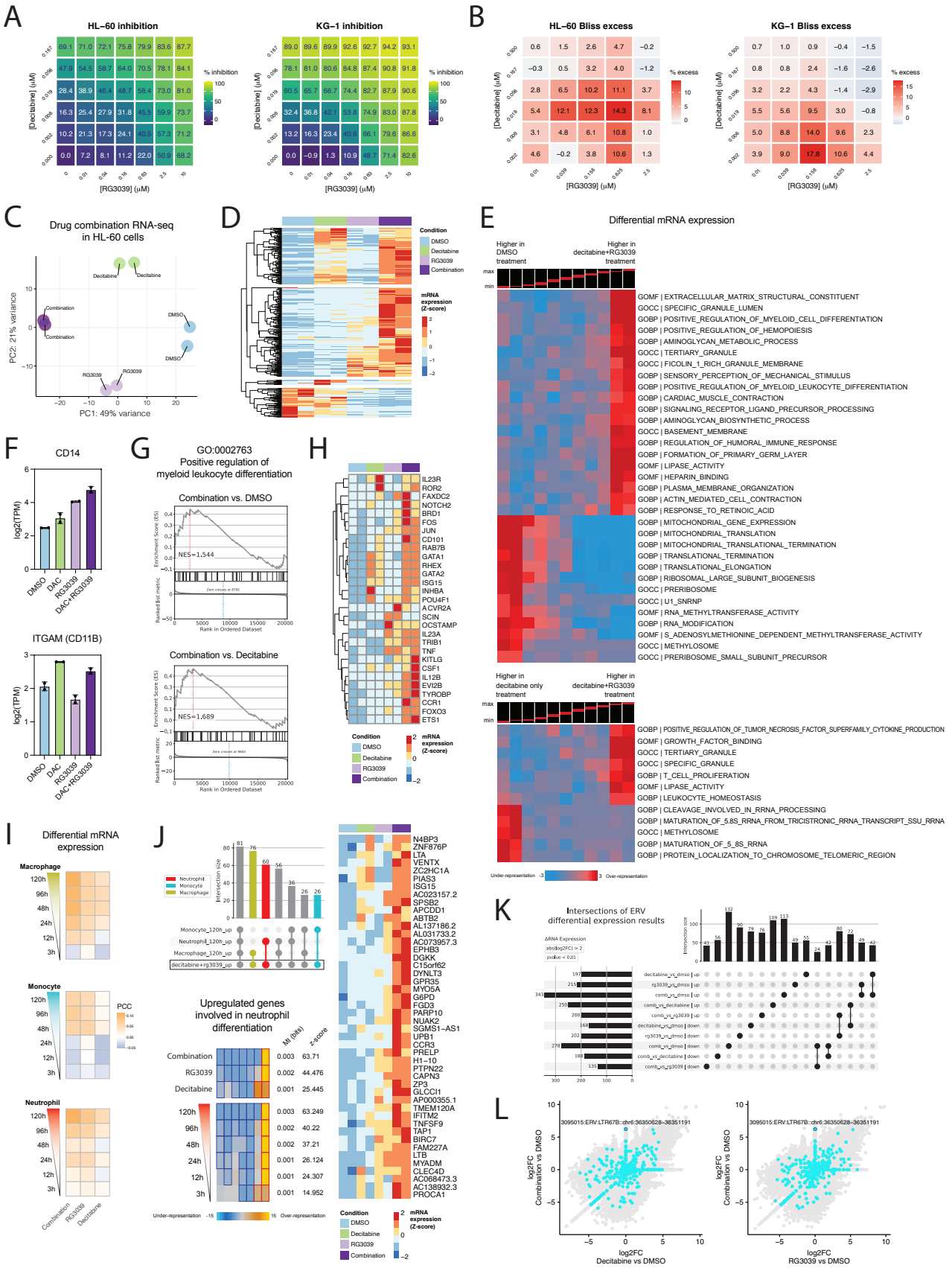

(**a**) Dose response matrices for HL-60 and KG-1 treated with dose combinations of decitabine and RG3039. Heatmaps display % cell inhibition (generated using a CellTiter-Glo assay; see methods for calculations) at each dose combination. Data are shown as means of two replicates. (**b**) Bliss excess scores (i.e., observed % cell inhibition – predicted % cell inhibition assuming Bliss independence; see methods for calculations) at each dose combination. Data are shown as means of two replicates. (**c**) PCA analysis of 3' RNA-seq (in duplicate) performed on HL-60 treated with DMSO, decitabine alone, RG3039 alone or both drugs. (**d**) DESeq2 analysis of 3' RNA-seq data reveals differentially expressed genes. Data are shown as a heatmap displaying counts row-normalized into Z-scores. (**e**) iPAGE analysis shows enrichment of gene ontologies (GOs) (heatmap rows) among differentially expressed genes (heatmap columns) in HL-60 treated with decitabine and RG3039 (top) or decitabine alone (bottom) vs. DMSO. Genes were first ranked based on log2FC from left to right and divided into eleven equally populated bins. Red boxes show enrichment and blue boxes show depletion. For each comparison, GOs are only shown if two of the first (i.e., upregulated GO) or last (i.e., down regulated GO) bins scored above 2. (**f**) Normalized RNA-seq counts for differentiation markers *CD14* and *CD11B* in HL-60 cells treated with DMSO, decitabine, RG3039, or decitabine plus RG3039. Data are shown as means of two replicates. (**g-h**) Expression patterns for genes involved in positive regulation of myeloid leukocyte differentiation (GO:0002763). (**g**) GSEA plot shows enrichment of the GO:0002763 term in the combined drug treatment (decitabine plus RG3039) relative to DMSO or decitabine alone. Normalized enrichment scores (NES) were calculated using the blitzGSEA Python package. (**h**) Normalized counts for genes in GO:0002763 upregulated upon decitabine and RG3039 treatment. (**i**) Treatment with decitabine plus RG3039 is more highly correlated with macrophage, monocyte, and neutrophil differentiation transcriptional signatures (derived from the public dataset GSE79044) compared to treatment with either drug alone. Data are shown as correlation matrices with Pearson's correlation coefficients (PCC). (**j**) An UpSet plots visualizes genes upregulated upon combined treatment with decitabine and RG3039 (top). PAGE analysis was performed to test for enrichment of genes involved in neutrophil differentiation, with results shown as a heatmap with rows as each logFC input and columns as cluster bins (bottom). Normalized counts for select genes most highly upregulated in the combination treatment (right). (**k**) An UpSet plot visualizes upregulated and downregulated endogenous retroviruses (ERVs) across treatment conditions. Upregulated ERVs (log2FC > 1 and p-value < 0.05) are labeled as "up", downregulated ERVs (log2FC < −1 and p-value < 0.05) are labeled as "down" and all other ERVs are labeled as "no change". (**l**) Scatter plots show differential ERV expression (as log2FC) in cells treated with decitabine or RG3039 alone (x-axis) vs. both drugs (y-axis). Pseudoautosomal boundary-like A (PABL_A) family members are highlighted in light blue. The labeled points correspond to the PABL_A chr9:9641512-9642657 locus, which is only upregulated in the decitabine and RG3039 drug combination.

Supplementary Figure 4. MeRIP-seq workflow to identify differentially methylated peaks associated with decitabine treatment in HL-60 cells

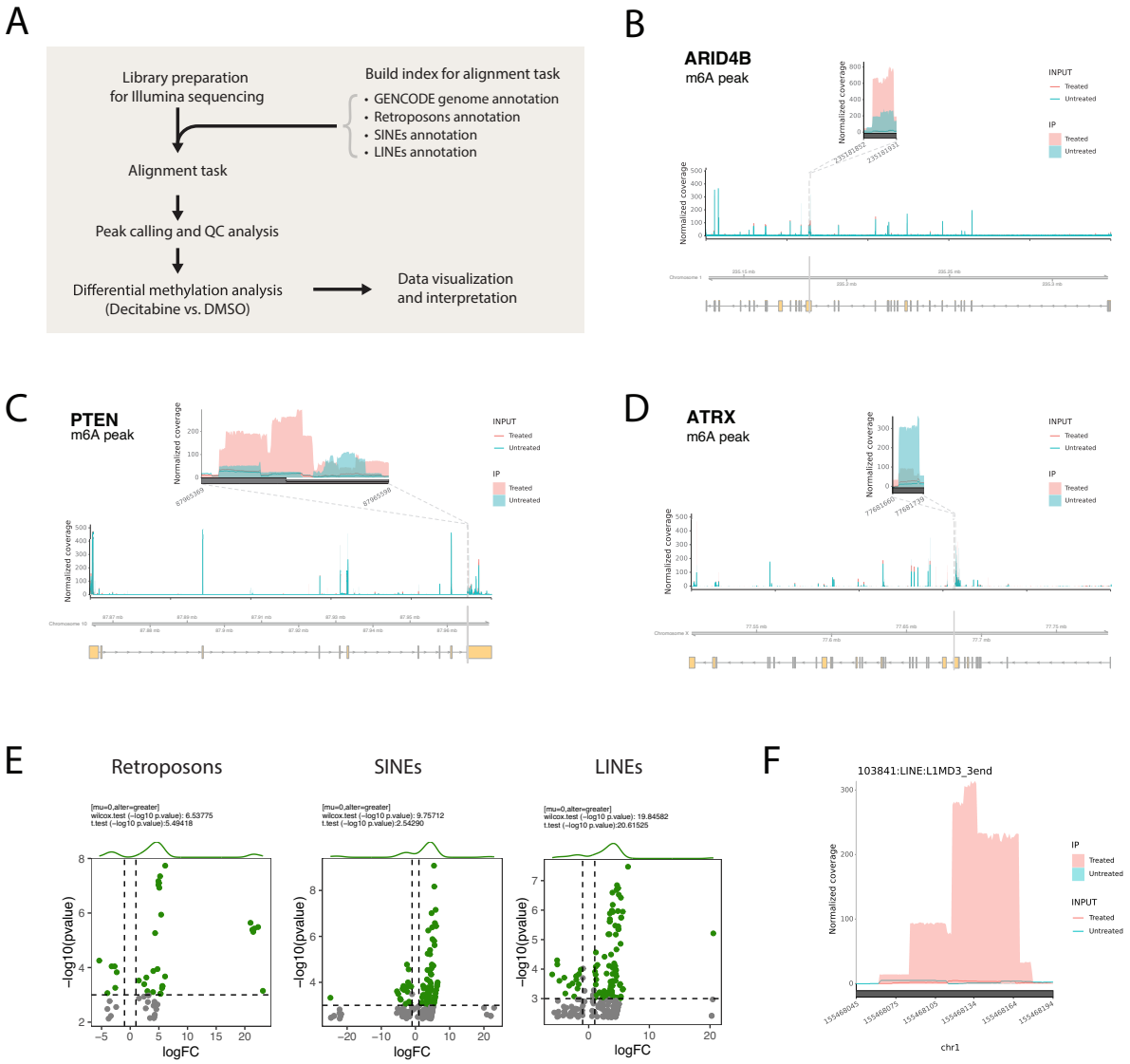

(**a**) Schematic of MeRIP-seq computational workflow. (**b-d**) Visualization of m^{6}A peaks across mRNA transcripts of **(b)** *ARID4B*, **(c)** *PTEN* and **(d)** *ATRX*. Peaks were called using the RADAR algorithm and plots were generated using the RADAR and Gviz R packages. MeRIP-seq experiments were performed in biological duplicates for each condition. **(e)** Differential methylation analysis shows significant changes in RNA methylation peaks in HL-60 cells treated with decitabine relative to DMSO. Global hypermethylation is observed in the decitabine condition for different families of ERVs. Peaks are called using the RADAR algorithm and visualized as annotated volcano plots. Wilcoxon and t-tests are used to assess statistical significance of global hypermethylation. **(f)** Coverage plot for a representative hypermethylated peak in the L1MD3_3end LINE transcript upon decitabine treatment (pink) compared to DMSO control (blue).

Supplementary Figure 5. Pathway-level changes in mRNA expression and stability associated with decitabine treatment in HL-60 cells

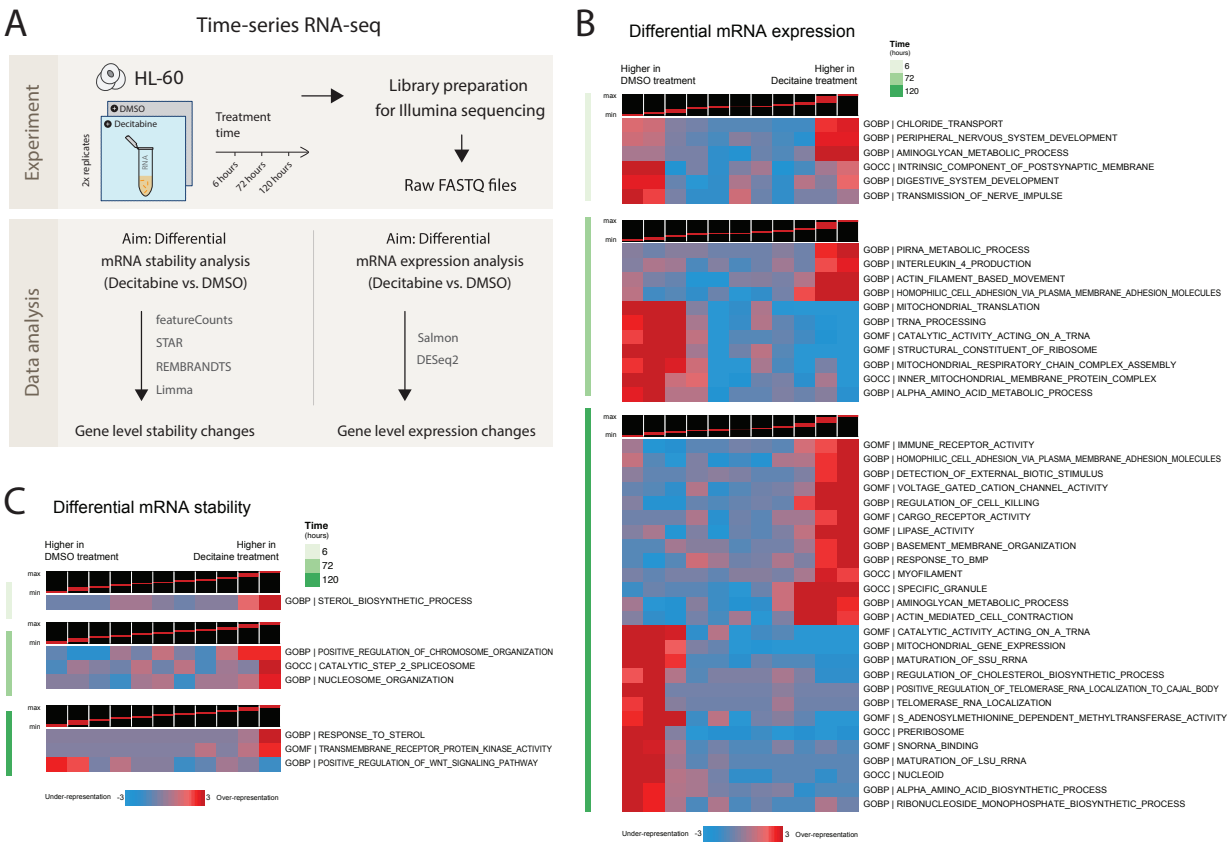

(**a**) Schematic of RNA-seq workflows in HL-60 cells. Two parallel workflows describe analysis of differential mRNA stability (left) and differential mRNA expression (right). (**b-c**) Gene set enrichment analysis with the iPAGE algorithm shows enrichment of GOs (heatmap rows) among changes in (**b**) RNA stability and (**c**) gene expression (heatmap columns; ranked and quantized into equal bins) upon decitabine treatment. The logFC values for HL-60 cells treated with decitabine vs. DMSO at 6 hours (top), 72 hours (middle) and 120 hours (bottom) were assessed separately. Highly-enriched GOs with genes upregulated or downregulated upon decitabine treatment are shown.

Supplementary Figure 6. Translational efficiency (TE) changes associated with decitabine treatment in HL-60 cells

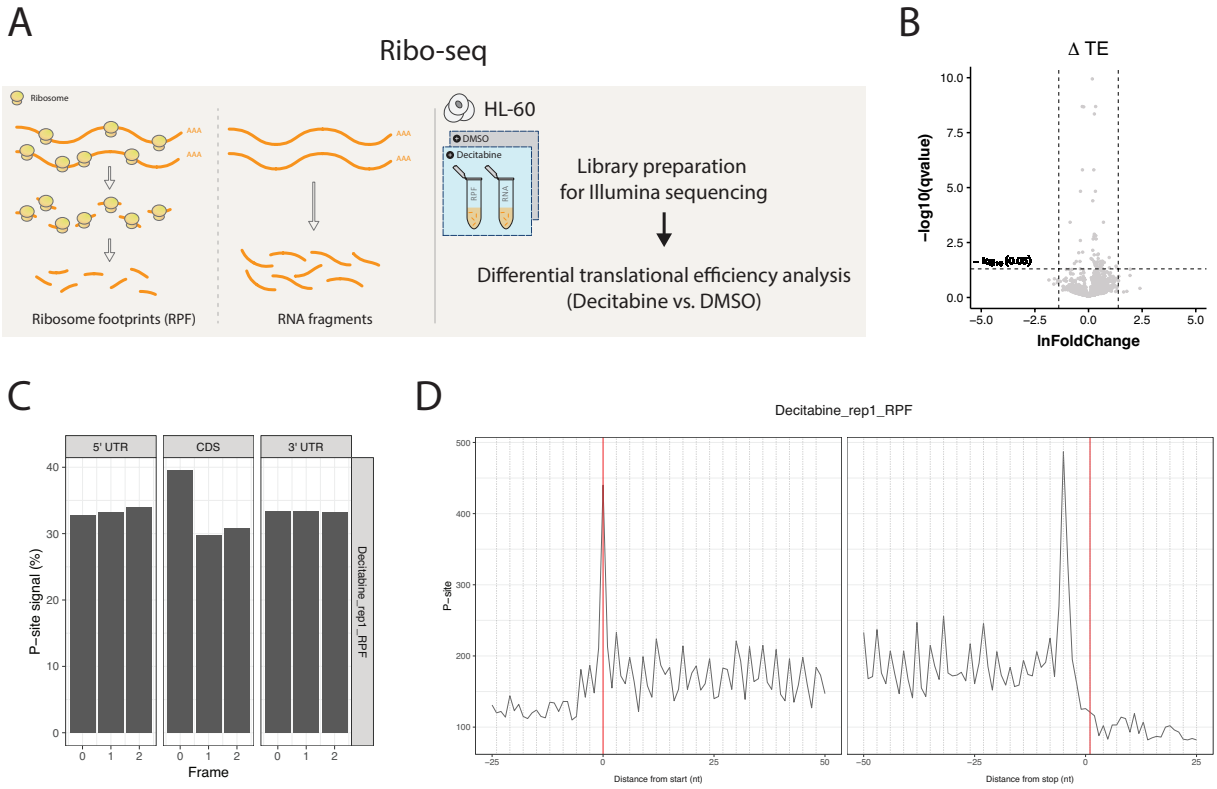

(**a**) Schematic of Ribo-seq experimental workflow. (**b**) Volcano plot visualization of Ribolog-calculated translational efficiency ratios (TERs) between the decitabine and DMSO conditions. (**c**) Bar plots showing enrichment of P-sites in the first frame of coding sequence (CDS) but not UTRs, consistent with ribosome protected fragments derived from protein coding mRNAs. (**d**) Ribosome occupancy profiles based on the 5' and 3' reads mapped to a reference codon for one sample (decitabine treated HL-60, single replicate).

Supplementary Figure 7. RNA m^{6}A hypermethylated peaks from MeRIP-seq in HL-60 following decitabine treatment

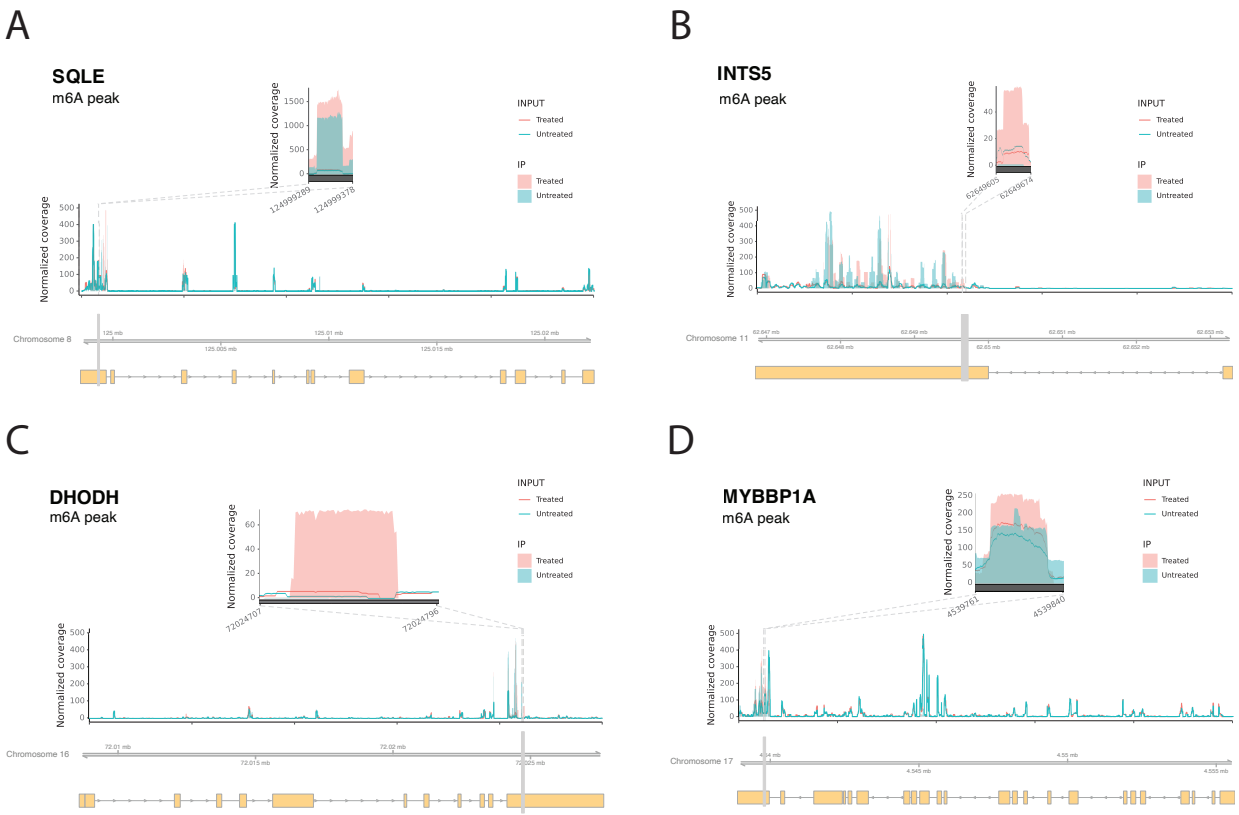

(**a-d**) Visualization of m^{6}A peaks across mRNA transcripts of **(a)** *SQLE*, **(b)** *INTS5*, **(c)** *DHODH* and **(d)** *MYBBP1A*. Peaks were called using the RADAR algorithm and plots were generated using the RADAR and Gviz R packages. MeRIP-seq experiments were performed in biological duplicates for each condition.

Supplementary Figure 8. Analysis of SKM-1 and MOLM-13 cell lines and genome-scale CRISPRi decitabine screens: quality control and comparisons to the HL-60 screen.

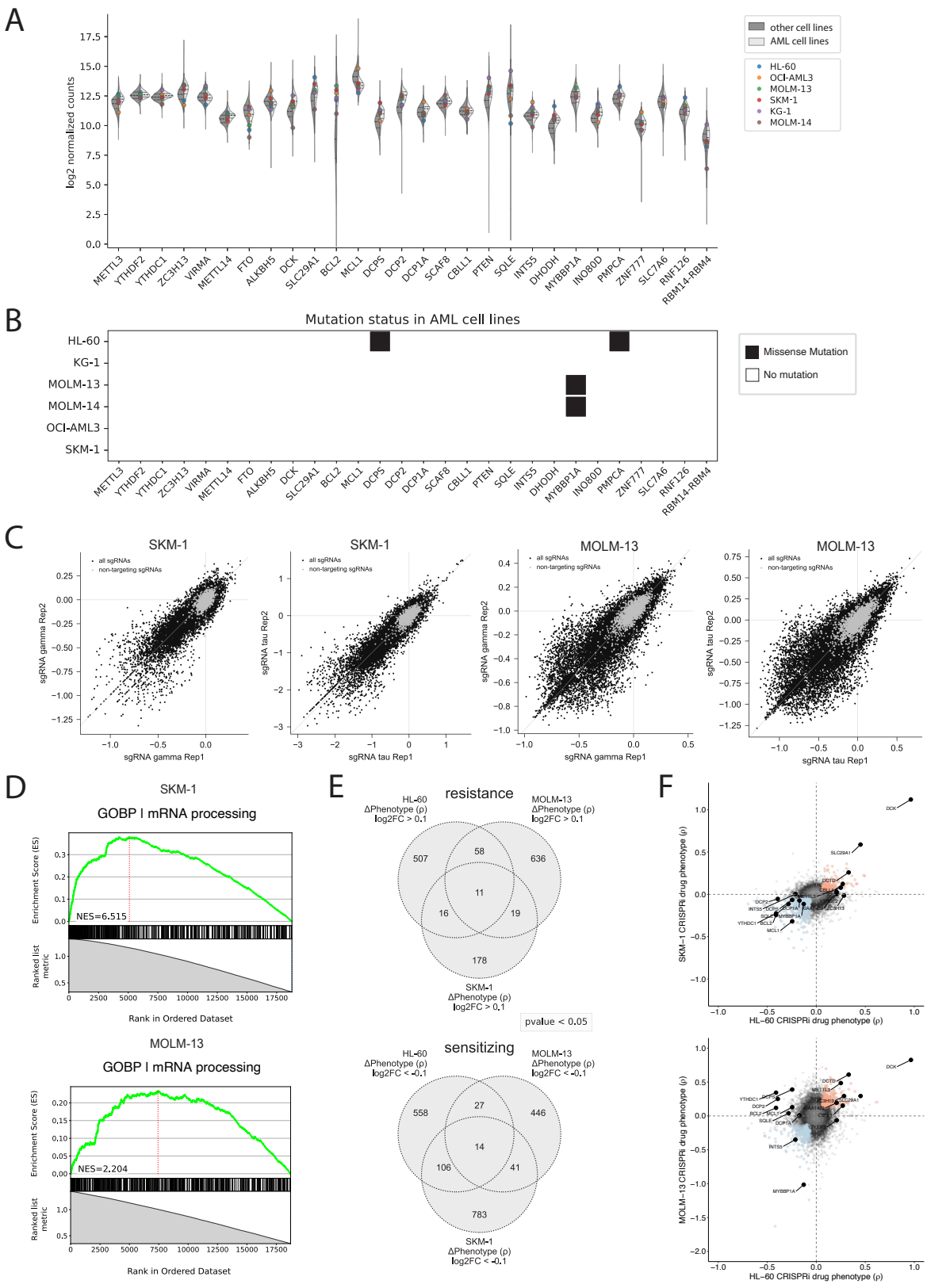

(**a**) RNA expression levels for genes of interest (shown as log2 normalized counts) across AML cell lines vs. other cancer types using the CCLE database (DepMap Public 21Q4) curated with Cancer Data Integrator (CanDI). In total, 54 AML cell lines and 1,771 other cancer type cell lines are shown, with the 6 AML cell lines used in this study highlighted. (**b**) Mutational status of genes of interest across the 6 AML cell lines used in this study. (**c**) Scatter plots show robust correlation between replicates for the gamma and tau phenotypes in SKM-1 (left) and MOLM-13 (right) genome-scale CRISPRi decitabine screens. (**d**) GSEA plots for the SKM-1 (top) and MOLM-13 (bottom) screens show enrichment of the GO:0006397 (mRNA processing) term among all screened genes ranked by Mann-Whitney p-value (corresponding to each gene's ρ phenotype calculation). Normalized enrichment scores (NES) were calculated using the blitzGSEA Python package. (**e**) Venn diagrams of significant hits across screens in three AML cell lines show overlapping and cell-line specific resistance (top) and sensitizing (bottom) phenotypes. Hits were selected by absolute gene-level rho (ρ) score values above 0.1 and Mann-Whitney p-values less than 0.05. (**f**) Scatter plots of gene-level rho (ρ) scores comparing the HL-60 screen to the SKM-1 (top) and MOLM-13 (bottom) screens. Several hits of interest shared across cell lines are labeled in black.

Supplementary Table 1. HL-60 CRISPRi decitabine screen
Gene-level phenotype scores and sgRNA protospacer sequences for validation assays.

Supplementary Table 2. Pathway-level analysis of HL-60 CRISPRi drug phenotype scores
Gene set enrichment analysis (GSEA) results using gene ontology (GO) gene sets. Two distinct GSEA analyses were performed (see methods).

Supplementary Table 3. Differential RNA methylation analysis
Differential analysis of MeRIP-seq data with RADAR (decitabine vs. DMSO).

Supplementary Table 4. SKM-1 and MOLM-13 CRISPRi decitabine screens
Gene-level phenotype scores for each screen and comparison of CRISPRi drug phenotype across three AML cell lines.

Supplementary Table 5. Pathway-level analysis of AML cell lines CRISPRi drug phenotype scores
Merged results from gene set enrichment analysis (GSEA) using gene ontology (GO) gene sets across three AML cell lines. Two distinct GSEA analyses were performed (see methods).